

TECHNOLOGY DEVELOPMENT FOR EXOPLANET MISSIONS

Technology Milestone Whitepaper

JPL Document D-81165

VERIFYING DEPLOYMENT TOLERANCES OF AN EXTERNAL OCCULTER FOR STARLIGHT SUPPRESSION

PROF. N. JEREMY KASDIN
PRINCIPAL INVESTIGATOR
PRINCETON UNIVERSITY
MECHANICAL AND AEROSPACE ENGINEERING

October, 2013

CoInvestigators:

David N. Spergel (Science PI), Robert Vanderbei, Princeton University; Stuart Shaklan (Institutional PI), Doug Lisman, Mark Thomson, Jet Propulsion Laboratory; Geoff Marks, Amy Lo, Northrop Grumman Astronautics; Bruce Macintosh, Lawrence Livermore National Laboratory.

Other Key Personnel:

Eric Cady, David Webb, Jet Propulsion Laboratory

Approvals

Released by:



10/15/2013

N. Jeremy Kasdin
Principal Investigator, Princeton University

Approved by:



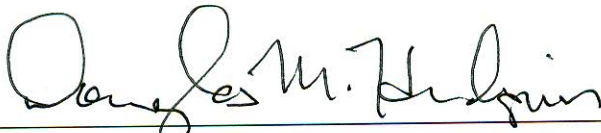
10/29/2013

Peter R. Lawson
Exoplanet Exploration Program Chief Technologist, JPL



10/29/2013

Gary Blackwood
Exoplanet Exploration Program Manager, JPL



11/13/13

Douglas Hudgins
Exoplanet Exploration Program Scientist, NASA HQ



11/13/13

Anthony Carro
Exoplanet Exploration Program Executive, NASA HQ

CONTENTS

1. Objective	4
2. Error Budget	5
3. Mechanical Design	6
3.1. System Description and Deployment Sequence	7
3.2. Petal Shape Design	9
3.3. Petal Mechanical Design and Development	11
3.4. Prototype Truss Design and Development	13
3.5. Prototype Hub Design and Development	15
3.6. Petal-Truss Interface Design	15
4. Deployment Test and Metrology	16
4.1. Deployment Testing	16
4.2. Metrology	17
4.3. Test Risks	18
5. Milestone Description and Data Analysis	18
5.1. Systematic Error	19
5.2. Random Error	19
6. Success Criteria	20
7. Certification	21
8. List of Acronyms	21
References	22

1. OBJECTIVE

A major science goal of the exoplanet research community is the detection and characterization of Earth-like planets. It is a central component of the NASA strategic plan and one of the top three science objectives in the ASTRO 2010 decadal survey. Nevertheless, doing so is a formidable task; planets are much fainter than their host stars and are often at small angular separations. In particular, Earth-like planets—that is, rocky planets in habitable zones—are estimated to be 10^{10} times dimmer than the stars they orbit and to be located at angular separations of a hundred milliarcseconds or less from the closest stars. Many approaches have been suggested over the last couple of decades for imaging these planets, including nulling interferometers, both structurally connected and free-flying, pupil interferometers, various types of coronagraphs, and external occulters. All have their advantages and disadvantages and all are at various levels of technological readiness. An important objective of NASA’s exoplanet program is to advance the technological readiness of the most promising approaches for exoplanet imaging so an informed choice can be made later this decade and progress can begin on an integrated observatory design.

We focus in this project on external occulters for achieving the needed starlight suppression. Our goal is to provide NASA with a viable low risk mission option that will be ready for mission development later in the decade. To that end, we have been performing technology development on all critical aspects of occulter development. In this successor Technology Development for Exoplanet Missions (TDEM) project, part of the ROSES Strategic Astrophysics Technology program, we further advance the technology by demonstrating precise deployment of a prototype starshade, raising the technology readiness level (TRL) of the critical deployment subsystem to TRL 4.

There are many challenges associated with starshade development and use. Most critical are 1) manufacturing an occulter to the required shape and meeting precise tolerances, 2) manufacturing the petal edges with small enough radius of curvature to minimize sunlight scatter into the telescope, 3) deploying the occulter central disk and petals while meeting the tight positioning requirements, 4) understanding and controlling the thermal deformations of the petals across the mission lifetime, and 5) demonstrating that the occulter can be precisely aligned with the telescope during an observation. We just completed a first TDEM project (TDEM-1), addressing the first of these, showing that an occulter petal can be built to the required tolerances, and measured, consistent with an overall contrast of 10^{-10} [1]. The second and fourth are currently being addressed in separate projects at JPL and subcontractors while the last is being investigated at Princeton University.

In this TDEM, as described in this whitepaper, we focus on challenge (3). We will develop a starshade system prototype, consisting of 4 of 30 petals attached to a slightly modified existing truss with a custom manufactured hub. Four petals are sufficient to verify petal interfaces and interactions and retire a large fraction of the deployment-related risks. We will use this prototype to demonstrate the deployment function and verify that deployed rigid-body position tolerance specifications are satisfied on a repeatable basis. The petals are scaled down and slightly modified versions of the TDEM-1 petal so that they match the existing truss (their design is described in Section 3.3). Our specific targeted milestone for this second successor TDEM can be succinctly stated:

TDEM Occulter Milestone:

- Verify that the deviations of the petal base point from the design circle are repeatedly below the 3σ positioning requirement for a 10^{-9} contrast using a sufficient number of deployments to verify the requirements are met with 90% confidence.

This milestone will demonstrate that the full system deploys in a well-behaved manner and to the required accuracy. We will use conventional photogrammetry to measure the deployed

position. Our specific metrics and success criteria are described in Section 6. The milestone also demonstrates that deployed position tolerance specifications are met in repeatable fashion. These specifications derive from an error budgeting tool that converts each error source into its contribution to instrument contrast. This same tool has been used to develop the error budget and shape requirements used for the milestone and success criteria in TDEM-1 and is described in detail in our final report.[1] A summary of the error budget is given in Section 2.

2. ERROR BUDGET

From our TDEM-1 study of petal construction errors [1], our starshade error budget studies [2, 3], and our analyses of likely truss deployment errors, we have constructed several error budgets for the detection of a planet having a contrast of 10^{-10} using a starshade with different size telescopes and different inner working angles. Our error budgeting calculations are based on diffraction sensitivity analysis [4] of manufacturing, deployment, and formation flying errors, along with estimates of thermal and dynamics contributions, solar glint, and reserve. Table 1, from [3], shows a comparison error budget for a small scale mission using a 1.5 m telescope and a large, flagship scale mission from our THEIA study using a 4 m telescope for a net contrast of 1×10^{-10} . The smallest inner working angle reasonably possible for the 1.5 m starshade is 75 mas whereas with the larger THEIA telescope and starshade we can reach 60 mas. This table shows the tradeoffs in various requirements made to reach the desired tolerance level. The 90 mas IWA and 32 m diameter starshade for a 1.5 m telescope was used for setting requirements for our TDEM-1 study, though with a relaxed tolerancing for 10^{-9} contrast for the purposes of the milestone [1]. Our mission modeling has shown that such a mission, at 10^{-10} contrast, is capable of discovery and photometric characterization of Earthlike planets in the habitable zone.

TDEM-1 studied the ability to meet the petal manufacturing errors. For this TDEM we are only considering the deployment errors associated with the three in-plane degrees of freedom of the petals treated as rigid bodies: radial and lateral displacement and rotation. For the full performance of a full scale star shade, we found in those earlier works, as shown in Table 1, that the radial (with respect to the center of the truss) and lateral (tangential to the truss) positioning tolerance requirements for the petal base attachment points were +/- 0.5 mm in plane. Though not shown in Table 1, the rigid-body angular rotation requirement for 10^{-10} contrast is ± 0.5 mrad.

In our current study, the truss diameter is 12 m and the contrast requirement is 10^{-9} . Since we expect, from simple geometry arguments, that the lateral and radial deployment errors for the smaller truss will scale linearly and thus be smaller than expected for the full scale model, we reduce the petal placement requirements by the truss diameter ratio (0.6). We also scale our tolerances by the square root of the contrast ratio (3.16) because deployment errors, and any other perturbations that cause local electric field errors, scatter light in proportion to the square of the perturbation amplitude. This leads us to a requirement of $\pm 0.5 * 0.6 * 3.16 = \pm 0.95$ mm on the radial and lateral in-plane position of the petal base points with respect to their ideal positions. The in-plane angular rotation requirement of the petal does not change with scale but does with contrast, making it ± 1.67 mrad.

Table 2 shows the resulting error budget for detection of a 10^{-9} contrast planet at the inner working angle of a starshade with a 12 m diameter truss. Only the deployment terms are tested in this TDEM. Our error budgets allow for global, random, and correlated errors. Global errors are common to all petals or truss bays, e.g., all petals are displaced outward by some distance from their ideal locations. Random deployment errors are uncorrelated between petal attachment points. We have modeled only one correlated errors to date, an in-plane elliptical deformation of the truss. A 1 mm elliptical deformation scatters about 50 times less light than a corresponding global petal displacement. Experience with the truss shows that its out-of-roundness is dominated by an elliptical deformation. These correlated errors are expected to be removed by the shimming process described in § 4.1. Future analyses will include higher-order shape terms.

Category	TDEM Design		THEIA Design		
	6 m petals, 23 m tip-to-tip 1.5 m diam. telescope		10 m petals, 40 m tip-to-tip 4 m diam. telescope		
	90 mas	75 mas	75 mas	60 mas	3-sigma
Manufacture					
Proportional width	10	5	10	10	ppm
Segment Placement	12.5	8	25	25	μm
Segment Shape	75	60	75	75	μm
Contrast	1.6×10^{-11}	1.5×10^{-11}	4.2×10^{-12}	8.9×10^{-12}	
Deployed Shape					
Proportional Width	5	5	5	5	ppm
Segment displacement	5	3.5	5	5	μm
In-plane quadratic bend	1	1	2	2	mm at tip
Out-of-plane quadratic bend	10	10	20	20	mm at tip
Contrast	2.0×10^{-12}	5.7×10^{-12}	3.1×10^{-13}	1.2×10^{-12}	
Deployed Position					
Radial shift	0.5	0.24	0.5	0.5	mm
Lateral shift	0.5	0.24	0.5	0.5	mm
Rotation about petal spine	0.25	0.25	0.25	0.25	deg
Elliptical truss deformation	1.00	0.75	1.00	1.00	mm
Contrast	2.2×10^{-11}	2.5×10^{-11}	1.3×10^{-11}	2.3×10^{-11}	
Thermal					
Proportional width	35	15	35	35	ppm
Base-to-tip gradient	15	15	15	15	ppm
Random local petal width	7.5	7.5	7.5	7.5	ppm
In-plane quadratic bend	1	1	2	2	mm at tip
Out-of-plane quadratic bend	10	10	20	20	mm at tip
Radial shift	0.2	0.13	0.2	0.2	mm
Lateral shift	0.2	0.13	0.2	0.2	mm
Contrast	1.3×10^{-11}	1.8×10^{-11}	4.8×10^{-12}	8.3×10^{-12}	
Formation Flying	1	0.25	1	1	m
Contrast	3.3×10^{-12}	4.5×10^{-12}	2.0×10^{-12}	4.7×10^{-12}	
Dynamics Allocation	5.0×10^{-12}	4.5×10^{-12}	2.0×10^{-12}	4.7×10^{-12}	
Edge Scatter Allocation	2.0×10^{-11}	2.0×10^{-11}	2.0×10^{-11}	2.0×10^{-11}	
Reserve	1.8×10^{-11}	6.8×10^{-12}	5.1×10^{-11}	2.9×10^{-11}	
Total	1.0×10^{-10}	1.0×10^{-10}	1.0×10^{-10}	1.0×10^{-10}	

TABLE 1. Flowdown of starshade tolerancing requirements for different missions scales for a total contrast of 10^{-10} at the inner working angle. (From [3].)

3. MECHANICAL DESIGN

Figure 1 shows a schematic diagram of our prototype starshade design fully deployed, consisting of a central hub (which would contain the spacecraft in a flight system), an expandable truss and up to 30 petals distributed around the truss. We describe the architecture in more detail in Section 3.1. Our plan is to build a $> 50\%$ scale prototype and perform deployment tests to verify compliance with deployment tolerance requirements. This prototype will consist of a full truss and 4 of 30 petals (as highlighted in Figure 1). Four petals are sufficient to demonstrate the petal-truss interface and any interactions between neighboring petals. The truss we are using is an existing demonstration unit that will be modified for: 1) mounting petals with latching hinge joints; 2) mounting to a

Category	Tolerance	Units
Manufacture		
Proportional width	19	ppm
Segment Placement	24	μm
Segment Shape	143	μm
Contrast	1.6×10^{-10}	
Deployed Shape		
Proportional Width	10	ppm
Segment displacement	10	μm
In-plane quadratic bend	2	mm at tip
Out-of-plane quadratic bend	19	mm at tip
Contrast	2.0×10^{-11}	
Deployed Position		
Radial base point position	0.95	mm
Lateral base point position	0.95	mm
Rigid-body rotation	1.67	mrاد
Attachment out-of-plane cylinder	4.00	mm
Out-of-plane displacement	25	mm at tip
Elliptical truss deformation	1.90	mm
Contrast	2.2×10^{-10}	
Thermal		
Proportional width	67	ppm
Base-to-tip gradient	29	ppm
Random local petal width	14	ppm
In-plane quadratic bend	2	mm at tip
Out-of-plane quadratic bend	19	mm at tip
Radial shift	0.38	mm
Lateral shift	0.38	mm
Contrast	1.3×10^{-10}	
Formation Flying	1.9	m
Contrast	3.3×10^{-11}	
Dynamics Allocation	5.0×10^{-11}	
Edge Scatter Allocation	2.0×10^{-10}	
Reserve	1.8×10^{-10}	
Total	1.0×10^{-9}	

TABLE 2. Flowdown of star shade tolerancing requirements for a total contrast of 10^{-9} at the inner working angle. Assumes a 12 m truss and 4.2 m petals.

central hub; and 3) replacing the parabolic dome-like structures needed for antennas with simpler spokes. The petal design consistent with the truss is described in Section 3.2.

3.1. System Description and Deployment Sequence. Figure 2 shows a representative occulter system in the stowed configuration, in this case mounted on top of a 1.1m telescope system, for a combined launch in a standard 5m launch fairing. This stowed view shows details of the spacecraft bus mounted inside of the starshade central hub, with protrusions for solar arrays, thrusters, antennas and attitude sensors. A perimeter truss forms the central disk. The truss is based on the AstroMesh reflector design developed by NGAS-Astro for antenna applications, with 7 successful missions to date. The truss is highly mass efficient and forms a stiff structure for the mounting of the petals. The truss perimeter is configured as flat faceted bays with one

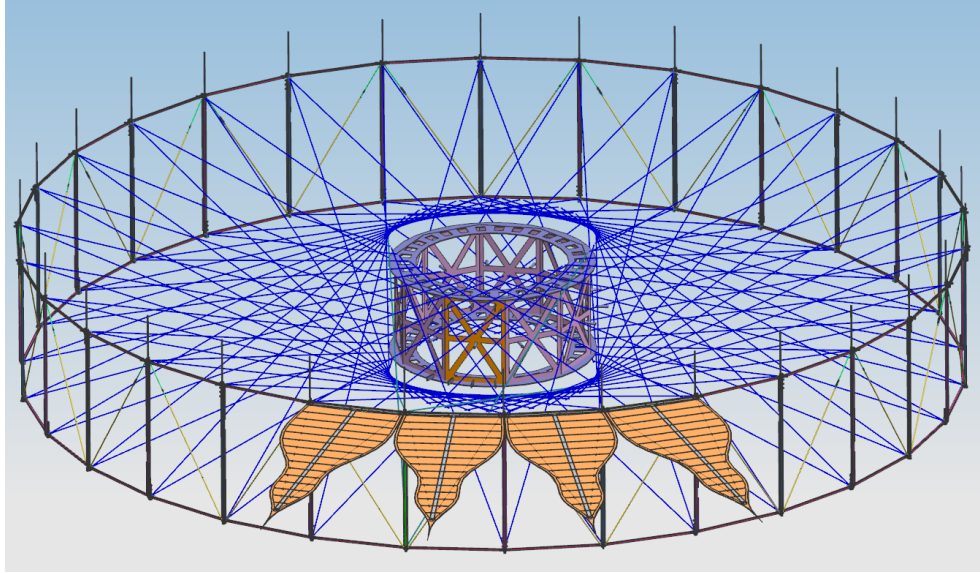


FIGURE 1. Prototype starshade architecture used for this TDEM test showing the central hub, spokes, truss, and four test petals.

petal mounted to each bay. An optically dark multi-layer fabric is loosely deployed over one surface of the truss. Tensioned spokes, which improve both truss stiffness and deployment accuracy, replace the parabolic dome structure that holds the RF mesh material to its required profile.

The petals are arrayed around the circumference of the truss with only three kinematic (statically determinate) interface points; two at the base and one that is provided by a pair of cords acting as stays, as on the mast of a sailboat. The petals employ a highly mass efficient lattice structure comprised of pultruded graphite fiber reinforced plastic (GFRP) rods and quasi-isotropic laminates that have finely tuned CTEs to limit thermal deformations. The petals wrap approximately 270° around the central hub. To avoid inelastic deformations with large margins, the hub diameter and petal structure is sized to limit strain rates below a maximum level of 0.5% with current estimates below 0.2%. The petals are covered on one side by an optically dark multi-layer fabric. The layers are spaced so that micrometeoroids do not create a stray light path, unless the particle trajectory is closely aligned with the direction of observation.

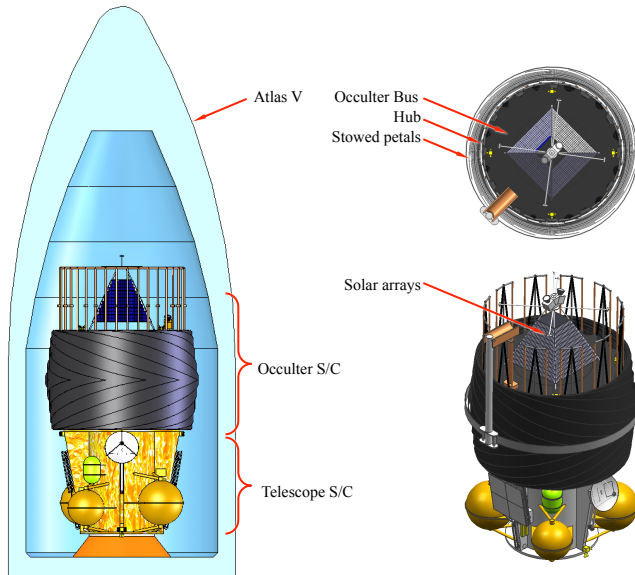


FIGURE 2. External occulter system in the stowed configuration



FIGURE 3. Starshade deployment stage 1—petal unfurling.

The starshade deploys in two stages. Figure 3 and Figure 4 schematically show the first and second stages of deployment, respectively (the petals in these figures are meant to represent a generic petal, not any specific design). The first stage unfurls the petals and occurs passively through the controlled release of stored strain energy. It is initiated by release of a belly-band restraint system around the circumference of the stowed starshade. The unfurling rate is controlled by a sequenced actuation of release devices to spool out lanyards. Once the petals are nearly straight a pair of spring-loaded ribs deploy towards the sun-facing side of the petal to stiffen it and maintain flatness.

The second stage deploys the truss and is accomplished by reeling in a deployment cable on a motor-actuated spool. The cable runs around the circumference of the truss inside the telescoping diagonal members, which are extended when stowed. Spooling in the cable forces the diagonals to retract, which deploys the truss. Each truss bay is synchronized to its neighbor by synchronizing gear pairs that are attached to adjacent longerons at every other truss node. The petals simply follow the truss as it deploys and complete a 90° rotation into the plane of the starshade. Near truss deployment completion, the petals are latched to the truss nodes. An animation of the entire deployment can be viewed at <http://planetquest.jpl.nasa.gov/video/15>.

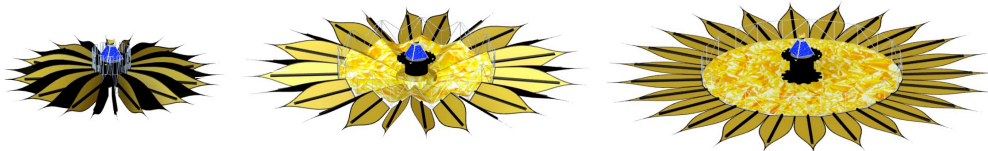


FIGURE 4. Starshade deployment stage 2—truss deployment.

Each petal is precisely located in-plane to maintain the global figure profile by two latches, one at each corner of the petal root. The latches provide kinematic restraint of the petal in all degrees of freedom, except rotation about the axis of the truss longeron adjacent to the root of the petal. The petals are aligned with the starshade plane with deployable stays that restrain the cantilever mode of motion. This produces a stiff tripod structure that is structurally efficient, as essential for achieving a high precision structure with low mass.

Figure 1 shows the planned prototype system with 4 out of 30 petals included. With a full complement of petals the tip-to-tip diameter is a little over 20 m, which is representative of an occulter that could detect Earthlike planets with a 1.5 m telescope.

3.2. Petal Shape Design. In our original conception, the petals for this deployment test were to simply be scaled down versions of our TDEM-1 project that fit the truss bays. However, because the number of bays differed and the resulting petals were not a consistent size for the given truss diameter, we opted instead to use our design tools to find a new design. This new design would result in a sufficient shadow were the prototype occulter with these petals to be operational with a 1.5 m telescope. The resulting petals have an unconventional shape because of the relatively large telescope diameter relative to the small occulter. While we could have opted for just the scaled down petals with no traceability to high contrast. However, redesigning demonstrates the flexibility of our design process and its ability to meet a variety of constraints. We thought it wise to test a

“real design” since there was no impact on manufacturing. We do concede that the error budget is based on the full scale, original petal design. It will be updated for the final report.

The shape of the petal edge is defined using a linear optimization, as has been done for all other petal shapes which have been built by JPL. To produce this, we begin with an integral representation of the electric field downstream of the occulter, under the assumptions of the Fresnel approximation and using a normally-incident plane wave on the occulter:

$$(1) \quad E_{\text{occ}}(\rho; \lambda) = E_0 e^{2\pi iz/\lambda} \left(1 - \frac{2\pi}{i\lambda z} \int_0^R e^{\frac{\pi i}{\lambda z}(r^2 + \rho^2)} J_0 \left(\frac{2\pi r \rho}{\lambda z} \right) A(r) r dr \right)$$

Here z is distance from the occulter to the telescope, λ is the wavelength of light, $i = \sqrt{-1}$, J_0 is the zero-order bessel function, E_0 is the constant input electric field from the star, E_{occ} is the electric field at the entrance aperture of the telescope (the shadow), and r and ρ are radial coordinates in the plane of the occulter and telescope aperture, respectively. The occulter is assumed to have a finite radius R , and the shape of its petals are defined by the apodization profile $A(r)$.

One major simplification is inherent in this representation: the binary nature of the petals is ignored. Eq. 1 represents the electric field from an apodized occulter whose apodization profile $A(r)$ changes with radius to match the fraction of a circle at that radius which is obstructed by petals. The full binary representation introduces a set of perturbation terms to this equation which have a negligibly small effect in a region near the optical axis. The size of this region depends on the number of petals, and for the simulated telescope diameters under consideration in this TDEM, 30 petals are more than sufficient to ensure that Eq. 1 is a good enough approximation for initial design purposes; the exact shape is used for verification in the final stages of design selection.

To optimize the occulter, we discretize r , ρ , λ , and $A(r)$ and write the following linear optimization, which minimizes the maximum excursion of the real and imaginary parts of the electric field:

$$(2) \quad \begin{aligned} &\text{Minimize : } c \\ &\text{subject to : } \quad Re(E_{\text{occ}}(\rho; \lambda)) - c/\sqrt{2} \leq 0 \\ &\quad \quad \quad - Re(E_{\text{occ}}(\rho; \lambda)) - c/\sqrt{2} \leq 0 \\ &\quad \quad \quad Im(E_{\text{occ}}(\rho; \lambda)) - c/\sqrt{2} \leq 0 \\ &\quad \quad \quad - Im(E_{\text{occ}}(\rho; \lambda)) - c/\sqrt{2} \leq 0 \\ &\quad \quad \quad c \geq 0 \\ &\quad \quad \quad \forall \quad \rho \leq \rho_{\text{max}}, \quad \lambda \in [\lambda_{\text{min}}, \lambda_{\text{max}}] \end{aligned}$$

(3)

where c is the desired contrast level, Re and Im denote the real and imaginary parts respectively, Typically, we then augment this with constraints on the derivatives of $A(r)$, as well as on the size of the tips of the petals and the gaps between petals.

For the petal in this deployment test, two additional constraints have been introduced to accommodate engineering considerations. First, a trapezoidal keep-out zone was defined to allocate space for the petal ribs to be installed without intersecting the edge. Second, a target region was chosen near the end of the petal through which the petal edge was required to pass. This constrained the width and length at the point where the edges end and the tip is to be installed. Fixing this length allows the composite face sheets for the petal to be made with existing equipment at JPL. As both of these requirements can be written as inequality constraints, the inequality matrices in the linear optimization were augmented and the optimization run with these requirements included.

The resulting petal, termed “GM4”, is shown in Fig. 5. Both of the additional regions of constraint are superimposed on the petal shape. The occulter is designed to provide 10^{-12} contrast

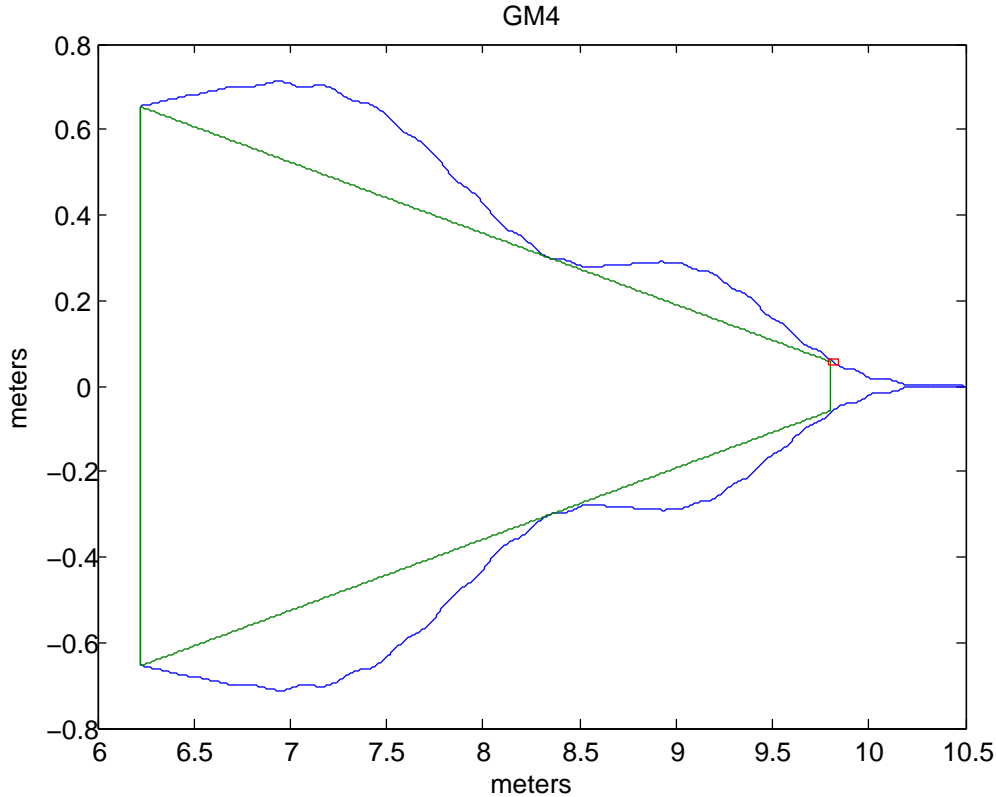


FIGURE 5. The shape of the petal for TDEM-2, shown in blue. The keep-out zone constraint, which ensures that there is space to mount the ribs, is shown in green, and the end target region, which fixes the length and end width of the structure prior to the tip, is marked in red. The optimization used to design the occulter shape required that the petal fall outside the green region and pass through the red one.

in the image plane beyond the 195mas geometric inner working angle (the 50% throughput point is at 149mas), over a 250-550nm bandpass. The occulter-telescope distance for this design would be 11,100 km. As explained earlier, the petal was redesigned to work with the smaller truss and provide traceability to the error budget. The smaller central disk results in these performance parameters, which are larger than we would design for a real mission. We do not intend to imply this is a flight design.

3.3. Petal Mechanical Design and Development. Figure 6 details the petal structural design, as developed for TDEM-1, as viewed from the sun facing, or anti-telescope side. Note that the petal in that figure has no particular high-contrast shape; it is a schematic to show the mechanical design approach. Not shown is an opaque thermal/optical blanket installed on the telescope facing side. The primary petal structure is a lattice construction with battens and longerons that intersect a longitudinal spine and a pair of structural edges on each side. The elements are optimized to place and precisely maintain the optical edges with the required profile over a wide range of operating temperatures. The lattice is highly mass efficient, yet very stiff in-plane. Secondary petal structure includes a pair of deployable ribs in an “A” frame configuration that stiffen and maintain overall deployed petal flatness. The deployable ribs fold outward and flat against the petal when stowed then pop up into place when the petal is unfurling. The ribs are deployed by extension springs that are inside hollow soda-straw size GFRP struts that lock the ribs in place at a

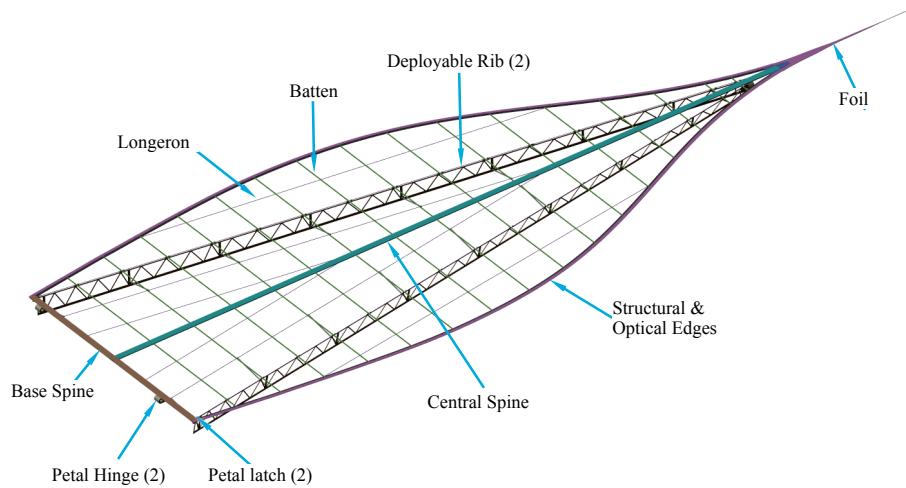


FIGURE 6. A schematic of a generic petal shape showing the important mechanical design details common to all petal shapes.

near-perpendicular angle to the petal when deployed. The ends of the deployable ribs coincide with truss-to-petal interface nodes on the base spine and with the outboard end of the outrigger at the apex of the “A” to complete the tripod-like geometry of the petal and outrigger support structure on the edge of the perimeter truss. The driver for sizing the ribs and battens is actually the 1-g compatibility requirement to limit petal deflections to less than 1 cm. The ability to perform sufficiently precise and repeatable starshade deployments on the ground ensures that truss and petal alignment verification can be performed with high confidence prior to launch.

Figure 7 shows photographs of the 7.25 m long proof-of-concept model (POC) that is close to full scale for the target mission with a 4 m UV telescope but without the precise optical edge shape. The petal includes a simplified opaque blanket, with only a single layer. Also shown in Figure 7 is a simulated central hub and a gravity compensation fixture (GCF). The POC petal has been used to verify the ability of a petal to passively unfurl, deploy its ribs and develop the required

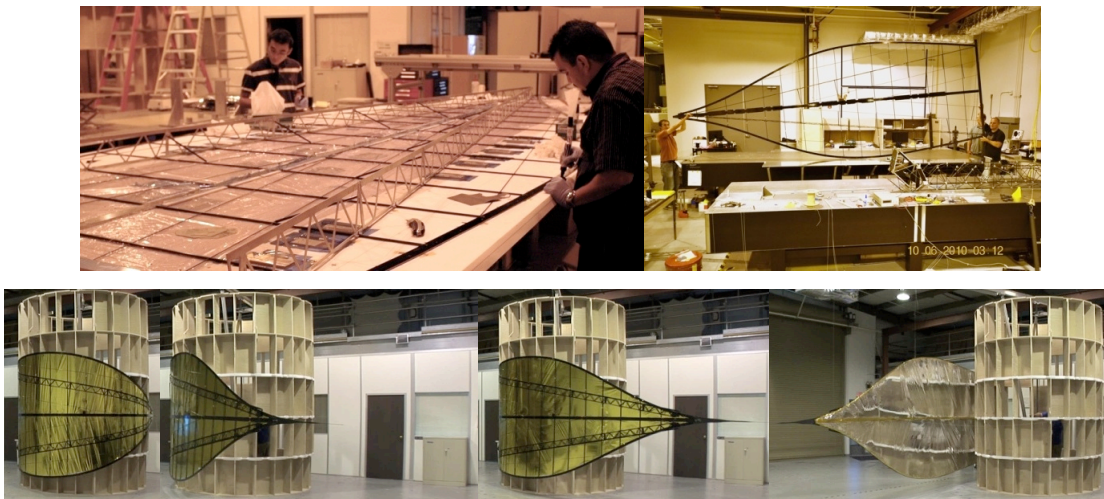


FIGURE 7. POC petal fabrication and deployment testing

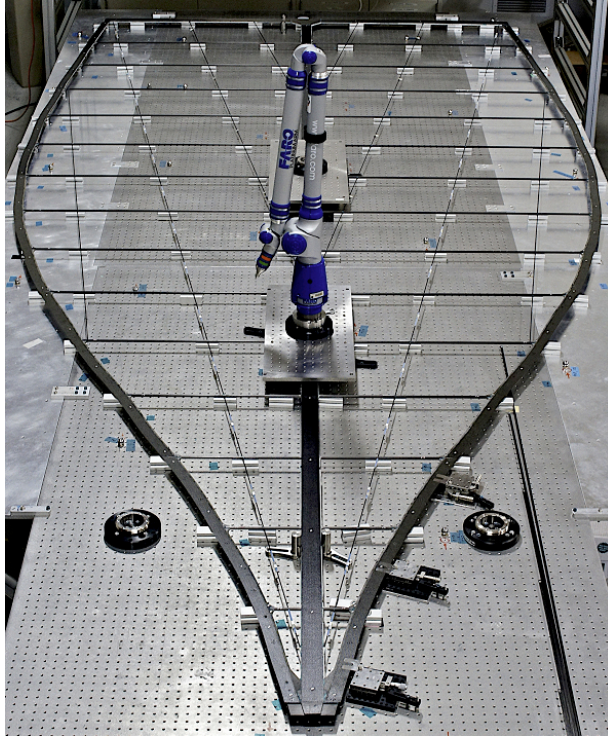


FIGURE 8. The final as-built petal completed during the first TDEM project on petal manufacturing and metrology.

high stiffness and overall flatness. This activity will be the first to integrate petals with a truss to produce a full starshade system prototype.

The POC petal design is flight-like but the construction is a hybrid of composite and aluminum materials that is appropriate for mechanical verifications only. It is being used as a testbed to develop new design elements and was an important tool for developing the designs for this TDEM project. A second generation breadboard petal, of all-composite construction, was constructed and measured as part of our TDEM-1 project on petal shape verification. A picture of the completed petal is in Figure 8. Details of the design and manufacturing process for that petal and the successful results of the metrology program can be found in the TDEM-1 final report.[1].

Similar to the POC petal, the petal mechanical design for this TDEM is representative of the previous TDEM-1 petal produced at JPL, but due to cost and schedule constraints, some non-flight materials are used. The battens and longerons are constructed of flight-like materials, but the structural edges, pop-up ribs, center spine and base spine include aluminum in their construction, rather than graphite. This is considered conservative for the purpose of this demonstration as the petal will be heavier than flight and there will be extra thermal deformations due to the higher CTE. Additionally, no optical edge is installed as this has no bearing on the deployment accuracy.

Finally, as explained earlier, the shape differs as the TDEM-2 petals were designed for the smaller central disk. Figure 9 shows 3 of these petals mounted to a hub mockup structure for deployment testing. Several stow and unfurl cycles have already been successfully demonstrated.

3.4. Prototype Truss Design and Development. Our TDEM deployment test will use an existing truss at Northrop-Grumman Astro that is slightly different (both in size and configuration) than the flight design prototype design described earlier. It is shown fully deployed in Figure 10. The truss is a graphite structure joined together with aluminum fittings and is approximately 12 m in diameter. This truss was originally used to demonstrate a modified deployment articulation that



FIGURE 9. Three petals mounted on hub mockup for preliminary deployment testing.

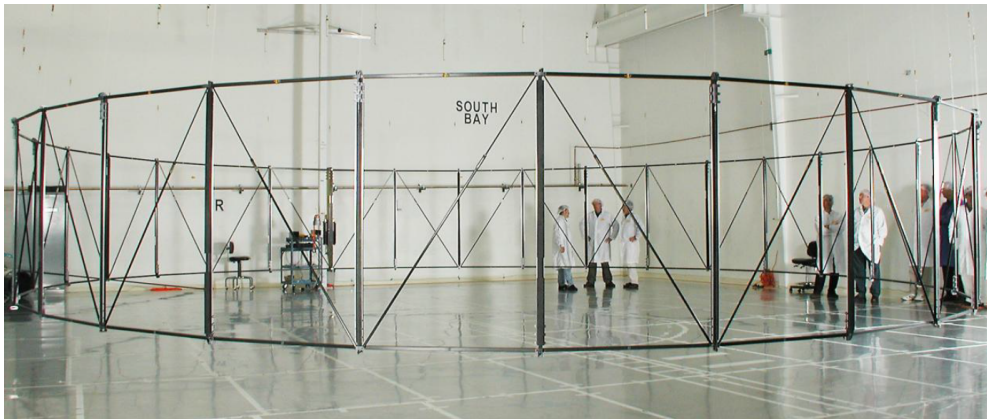


FIGURE 10. Existing truss model, fully deployed

stows more compactly than the original AstroMesh reflector design. The deployment kinematics of the available truss are not exactly the same as the version that would be used for the flight occulter, but for the purpose of this demonstration it provides the same interface to the petals and the same final deployed shape. As a result, it is a very cost effective means to demonstrate the feasibility of deploying occulter petals with the required accuracy, the purpose of this TDEM.

The structure that contributes to the required in-plane precision involves the spokes and the truss. The truss we are testing has longerons that are preloaded in compression by the spokes in the same way truss members in the flight design will be preloaded. They are made of the same materials as flight design and have the same number of pin hinges. The spokes are structurally representative, preloaded in tension to similar levels and are similarly anchored to a precision hub. Deployment errors will result from hysteretic behavior in the pin hinges, the longeron and spoke materials themselves, and errors due to inaccuracies in gravity compensation. Hysteretic behavior in the pin hinges will be minimal since they are all circumferentially preloaded. Hysteresis in the spokes and longerons will be minimal because of the constitutive properties of graphite composite.

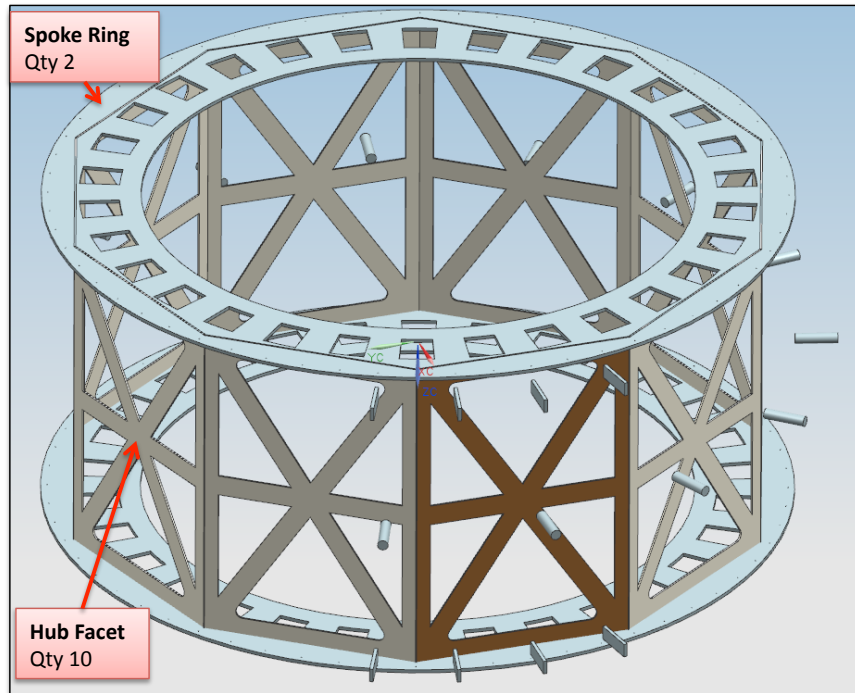


FIGURE 11. A schematic of the hub design.

In the flight design, the petals attach to truss longerons that need to be vertical in the stowed configuration to allow the petals to wrap around the hub. However, this existing truss is designed to stow down to 12 inches in diameter rather than the 3 m diameter needed for the starshade application. As a result, the longerons will not be vertically oriented when stowed around the hub. Our workaround for this is to mount the petals to the central hub directly when stowed. This allows functional testing of petal unfurling (not part of the TDEM milestone). After unfurling, the petals are manually remounted to the truss longerons. Truss deployment completes the rotation of the petals into the starshade plane. For flight the petals are directly mounted to the truss longerons, but they will not impart any loads into the longerons. This is because both the petals and the truss are also connected to the hub until after launch. Our plan is to perform several stow and unfurl cycles for the petals as a proof-of-concept of this design with multiple petals. After that the petals will be attached to the truss for the deployment tests and remain so for the remainder of the testing. This saves a significant amount of time, and thus cost, without detracting from the value of the TDEM milestone test.

3.5. Prototype Hub Design and Development. The hub being built for this TDEM test will be similar in concept to that shown in Figure 2 for a space system but custom designed and sized for the existing truss; a schematic of the hub design is shown in Figure 11. It is of aluminum construction and includes an upper and lower deck. Each deck has a ring of precisely positioned spoke attachment points. The hub is mounted to a wheeled undercarriage that will move on a floor mounted rail system, for the reason detailed in section 4.1.

3.6. Petal-Truss Interface Design. The petals mount to the truss longerons with precision pinned tabs and clevis joints. The deployment tolerance milestone applies to petal attachment points and more specifically the center of each interface joint. This center point will be precisely characterized relative to petal mounted targets using photogrammetry. Figure 12 shows the truss stowed and attached to the hub with the petals attached to the longerons ready for deployment.

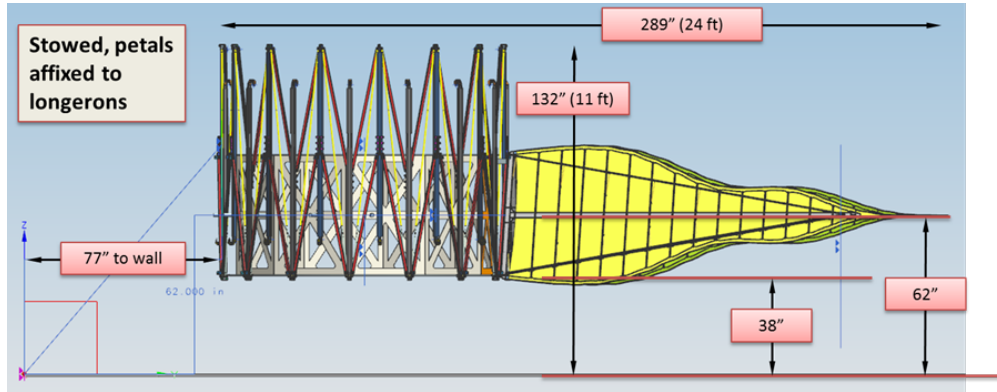


FIGURE 12. A schematic of the stowed truss with the petals attached at an angle on the longeron ready for deployment.



FIGURE 13. Existing truss gravity compensation fixture (GCF).

4. DEPLOYMENT TEST AND METROLOGY

This section details the planned testing, test equipment required, metrology approach and data analysis approach.

4.1. Deployment Testing. Deployment testing is performed at the Northrop Grumman Astro facility in Goleta, California, dedicated to Astromesh antenna testing. Figure 13 shows the existing gravity compensation fixture (GCF) that will be used that will be realigned for off-loading our circular truss rather than the slightly elliptical Astromesh antennas. The truss GCF consists of a set of fan shaped rails with low friction trolleys and counterweights on pulleys. Astromesh antennas deploy outward in one direction, but the starshade truss deploys radially outward in a symmetric fashion. For this reason, the hub is rolled out on a track system to stay positioned near the center of the truss.

The petals require additional GCFs for both the unfurling stage and the truss deployment stage. The GCF for unfurling consists of 4 separate swing arms, one for each petal. The swing arms are mounted at variable heights to a common post, which is mounted to the top of the hub. Each swing arm rotates to follow its petal while a single counter-weighted attachment line moves radially out on a low friction trolley. The variable arm heights allow the arms to pass over each

other. A rate controlled lanyard system is also used during unfurling to control and synchronize the unfurling of all 4 petals.

The petal GCF for truss deployment consists of additional rails mounted in between the truss GCF rails and extending further outward. As each petal is manually installed on the truss the GCF line is removed from the hub mounted system and connected to the overhead rail system. The hub is a rigid structure and targets mounted on the hub will be used as the reference point for co-registering the large number of petal and truss target position measurements.

We note that the GCF can apply unwanted forces that may cause distortions. In other words, the presence of the petals can affect deployment accuracy and repeatability through forces they impose via the GCF. However, If we can demonstrate the required repeatability with petals in a 1-g environment, we have conservatively demonstrated the required in-flight capability. We will have to demonstrate repeatability with petals installed on the flight hardware anyway; this is typical. If the requirements cannot be met, the next step is to evaluate the impact of off-loading errors on shape and improve the off-loading as needed.

The first phase of deployment testing will focus on the truss by itself with no petals installed. A number of deployments will be performed with the truss shape measured after each deployment to establish the truss repeatability. Knowledge of truss repeatability is useful both for diagnosing the full system results and guiding the test approach. For example, if truss repeatability is good, some, but not all, of the full system deployments can be performed without fully stowing the truss, which is a time consuming process. This in turn would allow additional deployment cycles improving the statistical confidence level.

The second phase of deployment testing is performed with the petals installed and will focus on characterizing the influence of petal stowing and unfurling on the deployed truss shape. If petal stowing and unfurling is found to have an acceptably small influence on truss shape repeatability, it may be possible to streamline the process and not remove the petals from the truss as part of each deployment cycle. Again, this allows additional deployment cycles and improves the statistical confidence level.

The third phase of deployment testing is performed with the petals and is focused on shimming the petal attachment interfaces to reduce any bias shape error. This will be an iterative process and require multiple deployment cycles as necessary to reduce the bias positioning error to an acceptable level. This will address local errors at the petal attachment points as well as global deformations based on measurements of the entire truss. The shimming control accuracy is expected to be better than 80 microns, combining the thickness of the shims and the measurement accuracy of the photogrammetry.

The fourth and final phase of deployment testing is focused on verifying the milestone specifications and no changes will be made to the petal interface shims. A minimum of 5 deployment and measurement cycles will be performed.

4.2. Metrology. All metrology is performed with an existing Geodetics V-Stars photogrammetry system. Each measurement is based upon approximately 30 separate photographs. The V-Stars system will be programmed to autonomously recognize designated targets on the hub as the reference bar and will establish the position of approximately 200 targets relative to this reference bar. The expected in-plane and out-of-plane position accuracy is about $75 \mu\text{m}$, which is less than 10% of the milestone specification of in-plane tolerance.

Each petal is equipped with 2 calibrated targets on either end of the base of the petal. The photogrammetry system measures the (x, y) in-plane (Cartesian) position of each target relative to a calibrated fiducial in the room. The fixed petal width provides a constraint so that the 4 translational measurements of each petal span the three degrees of freedom desired. The four base measurements of each petal are used to find a best-fit circle corresponding to the central disk of the occulter. Since the requirements are for absolute positioning of the petals relative to the designed

central circle, any radius deviation between the best fit circle and the design is an absolute bias error. The measurements are then processed to determine the radial and transverse deviations of each petal relative to the best fit circle as well as the rigid-body rotation of the petal; this scatter represent the repeatability of the deployment (plus the measurement error). To meet the milestone, the sum of the bias and the scatter must be less than the requirements described in Section 2. Section 5 describes the statistics associated with how these measurements are processed to determine the confidence in the milestone verification.

4.3. Test Risks. As with any new mechanical design and test procedure, there are various risks that, if realized, could result either in complete failure to deploy or a larger positioning error causing us not to meet our milestone. While we believe the probability of these events is small, we list here the top sources of risk to the TDEM test.

- If the metrology measurements are not properly calibrated or the photogrammetry and laser tracker do not converge to the extent that we cannot demonstrate the required performance, then this will require a recalibration and measurements will have to be repeated at additional cost and schedule or we will fail to meet the milestone.
- If the truss shape upon deployment has significant out-of-roundness, then the spoke lengths or GCF will require modification. This will affect cost and schedule and could impair ability to complete the test.
- If we designed an inadequate amount of adjustability in the petal interface shim stack to meet the absolute circularity requirement, then this would result in the truss being unusually out-of-round.
- If the truss-petal system hysteresis and GCF are inadequate, then the deployment positional repeatability will exceed requirements.
- If there are unexpected problems with deployment (like snags, spoke failure, GCF failure) then our schedule will extend and cause us to run out of funds.
- If a forklift or man-lift rams the test article or other safety problems occur during the assembly and test, then we could have total failure of the experiment.

5. MILESTONE DESCRIPTION AND DATA ANALYSIS

In Section 2 and Table 2 we described the error budgeting process and the allocated deployment requirements for a starshade consistent with 10^{-9} contrast. In particular, the two in-plane error terms being verified in this TDEM, the radial and lateral positioning of the root attachment point of the petal, must have an absolute position accuracy better than 0.95 mm. Likewise, the rigid body rotation of the petal must be less than 1 mrad. It is common aerospace practice to consider this a 3σ error bound. That means that the sum of any systematic bias in displacement plus the three standard deviations of the underlying deployment distribution must be less than this value. The error budget described in Section 2 separately allocates error for the systematic, correlated errors (namely the ellipticity of the truss) and the random errors in petal positioning. The verification process for this TDEM milestone is to take sets of measurements of the root positions and compare their mean and variance against thresholds for the systematic bias and variance to ensure that the requirement is met with 90% confidence:

TDEM Occulter Milestone:

- Verify that the deviations of the petal base point from the design circle are repeatedly below the 3σ positioning requirement for a 10^{-9} contrast using a sufficient number of deployments to verify the requirements are met with 90% confidence.

In this section we describe the process for determining those threshold values as a function of the requirements and the number of samples.

For the statistical analysis we ignore the measurement noise and consider only the random distribution of deployment error. Since the requirement on the positioning is of the order 1 mm and the expected measurement noise has a standard deviation of 75 μm , this is a good assumption and simplifies the analysis (note that the results are conservative, that is, including measurement noise would relax the resulting milestone requirement). We assume that the underlying probability distribution governing the deployment of the petal roots relative to the best fit circle is Gaussian with mean zero and variance σ^2 . We also assume that the distributions of radial, lateral, and angular errors are independent as are the distributions of each of the four petals. Since the requirement is on *absolute* positioning we also allow for a possible systematic bias in the deployed position, denoted b , though the assembly process is designed to make that zero. The requirement is then that $b + 3\sigma \leq 0.95$ mm for each of the radial and lateral distributions and $b + 3\sigma \leq 1$ mrad for the rigid-body rotation. For the remainder of this discussion we consider only the radial error; the analysis for the lateral and angular error is identical.

5.1. Systematic Error. Assuming n independent deployments, the measurement process described earlier provides n measurements of the absolute position of the root of each petal relative to a fixed fiducial. From that we calculate the best fit circle. The radius of that circle is the mean value of the measurements, which we denote \bar{X} . We then calculate the sample variance of the measurements relative to that mean radius, denoted s^2 .

Using the fact that the estimate of the mean is normally distributed, we can put confidence intervals around our estimate of the mean. In other words, for a confidence of $100(1 - \alpha)\%$, the true mean falls inside the interval

$$(4) \quad \left[\bar{X} - z_{\alpha/2} \frac{s}{\sqrt{n}}, \bar{X} + z_{\alpha/2} \frac{s}{\sqrt{n}} \right]$$

with $100(1 - \alpha)\%$ confidence, where $z_{\alpha/2}$ is the critical normal deviate. For 90% confidence, $\alpha = 0.05$ and $z_{0.05} = 1.64$.

Thus if the desired absolute mean (radius of the best fit circle) falls within the interval, we can say with 90% confidence that the distribution has the correct mean (i.e., there is no systematic error). Using the values from the next section for the threshold on the standard deviation, we can plug in $s = 0.22$ mm and find that the 90% confidence interval around the mean is 0.1 mm. Thus, if the measurement of the mean is more than 0.1 mm from the desired radius, then we must assume there is a systematic bias with 90% confidence. To ensure 90% confidence in our final criteria, we take the larger of the two bounds in the confidence interval for the systematic bias, $b = \bar{X} \pm z_{\alpha/2} \frac{s}{\sqrt{n}} - \mu$, where μ is the desired mean value (radius).

5.2. Random Error. Here we consider the random deviations of each measurement about the mean. First, we assume that there is no systematic error, $b = 0$. That is, the best fit circle has the correct absolute radius within the limits of the measurements and the only error source is random deviations of each petal from that during each stow-and-deploy. Since the 0.95 mm requirement is a 3σ bound, we require that the standard deviation of the underlying distribution of deployment error (with zero mean) be $\sigma \leq 0.95/3$ or $\sigma \leq 0.32$ mm. That ensures that there is a less than 0.1% chance that any given deployment (such as the final one in space) will exceed the required tolerance of 0.95 mm.

We confirm that the actual stow-and-deploy process being measured meets that requirement with 90% confidence through repeated stow and deploy tests and measurements of the displacement. We could do a goodness-of-fit test to ensure the distribution is what we want, but that would be quite difficult with such a small sample so we do a slightly weaker test to ensure that the real standard deviation, σ , is less than or equal to the required standard deviation with 90% confidence.

Suppose we take n measurements and form an estimate of the variance, s^2 . Then the $100(1 - \alpha)\%$ confidence limits on that estimate are

$$(5) \quad \frac{(n-1)s^2}{\chi_{\alpha/2}^2} \leq \sigma^2 \leq \frac{(n-1)s^2}{\chi_{1-\alpha/2}^2}$$

where χ^2 is the Chi-square statistic for $n-1$ degrees of freedom.

This lets us set the required bound on our estimate s^2 to give 90% confidence the true variance meets the requirement. In other words, for any given estimate s^2 , we know with 90% confidence only that the true variance σ^2 lies within the bounds $[\frac{(n-1)s^2}{\chi_{\alpha/2}^2}, \frac{(n-1)s^2}{\chi_{1-\alpha/2}^2}]$. In order to ensure that the real variance meets the requirement with 90% confidence, we set the threshold on our measurement from the upper bound of the interval, requiring that

$$(6) \quad \frac{(n-1)s_r^2}{\chi_{1-\alpha/2}^2} = \frac{D^2}{9}.$$

where $D = 0.95$ mm is the 3σ bound.

Thus, the threshold value is given by

$$(7) \quad s_r^2 = \frac{D^2 \chi_{1-\alpha/2}^2}{9(n-1)}.$$

As long as the sampled variance is below this threshold, we have 90% confidence that the 3σ bound on the underlying distribution has been met. Note that for small numbers of samples this can be a significant derating on the threshold, greatly tightening the requirements of the test.

Considering only a single petal and 5 stow-and-deploy tests ($n = 5$), Eq. 8 gives a threshold variance for the 0.32 mm bound, of 0.02 mm² (or a sample standard deviation of 0.13 mm). For this case, $\chi_{0.95}^2 = 0.711$. This requirement is relaxed if we assume that all three petals behave independently. We can then assume we have 15 measurements, making $\chi_{0.95}^2 = 6.6$ and the threshold variance 0.05 mm² (or a sample standard deviation of 0.22 mm).

If there is a systematic bias detected, then ensuring the same overall error meets the requirement means lowering the bound on the variance of the deployment distribution to compensate. In that case, the threshold test becomes

$$(8) \quad s_r^2 = \left(\frac{D^2}{9} - b \right) \frac{\chi_{1-\alpha/2}^2}{(n-1)}.$$

Of course, this is a much tighter bound on the measured variance.

6. SUCCESS CRITERIA

In TDEM-1, our success criterion was based on the ultimate contrast an occulter achieved. This had the advantage of being directly traceable to the requirements of an imaging mission. This criterion was established through a combination of metrology and modeling, using analysis of the measured data to make a prediction of the contrast from an occulter made from similar petals as that measured. This approach was sensible because of the large number of measurements made along the petal edges and the limitation of any error analysis that reduces those measurements to a small number of parametric terms. We thus came to a statistical estimate of the likely contrast.

In this second TDEM project, such an end-to-end analysis is not necessary. Here we have only a small number of measurements of three error parameters: the petal base point radial and transverse position and the petal rotation. These three error terms are directly traceable to contrast via the error budgeting process described in § 2. A detailed conversion to contrast as we did in TDEM-1 would be superfluous and unnecessarily cumbersome. We therefore establish success through the process described above, repeatedly measuring the petal positions after deployment, combining the measurements, and comparing to the 3σ requirements. This process can be summarized as follows:

- (1) Mount petals on truss.
- (2) Deploy truss with attached petals using the gravity offload fixture.
- (3) Measure the base targets of each petal relative to the fixed fiducial origin.
- (4) Perform fit to find best fit circle to base positions.
- (5) Process measurements to determine radial and transverse bias of circle and radial and transverse positions of each petal as well as in plane rotation.
- (6) Repeat steps 1-5 n times. Process the n measurements as described § 5 to determine best estimates of radial, transverse, and rotational errors with confidence intervals to determine if milestone requirement was met with 90% confidence.

7. CERTIFICATION

The PI will assemble a milestone certification data package for review by the ExEPTAC and the ExEP program. In the event of a consensus determination that the success criteria have been met, the project will submit the findings of the review board, together with the certification data package, to NASA HQ for official certification of milestone compliance. In the event of a disagreement between the ExEP project and the ExEPTAC, NASA HQ will determine whether to accept the data package and certify compliance or request additional work.

The milestone certification data package will contain the following explanations, charts, and data products:

- (1) A narrative report, including a discussion of how each element of the milestone was met, and a narrative summary of the overall milestone achievement.
- (2) Description of truss, hub and petal designs and materials and assembly steps.
- (3) Description of the photogrammetry metrology system and certification.
- (4) Description of the metrology process.
- (5) Description of the model fitting and data analysis process and results including error estimates and best fit circle biases.
- (6) Description of the milestone determination and certification.

8. LIST OF ACRONYMS

CTE	Coefficient of Thermal Expansion
GCF	Gravity Compensation Fixture
GFRP	Graphite Fiber Reinforced Plastic
IWA	Inner Working Angle
JPL	Jet Propulsion Laboratory
NASA	National Aeronautics and Space Administration
POC	Proof of Concept
TDEM	Technology Development for Exoplanet Missions
THEIA	Telescope for Habitable Exoplanets and Intergalactic Astronomy
TRL	Technology Readiness Level

REFERENCES

- [1] N. Jeremy Kasdin. Advancing technology for starlight suppression via an external occulter. Technology Development for Exoplanet Missions Final Report, JPL Document D-74384, September, 2012.
- [2] Stuart B. Shaklan, M. Charley Noecker, Tiffany Glassman, Amy S. Lo, Philip J. Dumont, N. Jeremy Kasdin, Eric J. Cady, Robert Vanderbei, and Peter R. Lawson. Error budgeting and tolerancing of starshades for exoplanet detection. volume 7731, page 77312G. SPIE, 2010.
- [3] S. B. Shaklan, L. Marchen, P. D. Lisman, E. Cady, S. Martin, M. Thomson, P. Dumont, and N. J. Kasdin. A starshade petal error budget for exo-earth detection and characterization. In *Proceedings of the SPIE Astronomical Instrumentation Conference*, number 38 in 8151, 2011.
- [4] E. Cady. Boundary diffraction wave integrals for diffraction modeling of external occulter. *Optics Express*, 20:15196–15208, July 2012.